Desalination and Water Treatment
www.deswater.com

doi: 10.1080/19443994.2015.1136963

57 (2016) 22646–22654
October

Taylor & Francis
Taylor & Francis Group

Adsorption of methyl red onto palladium nanoparticles loaded on activated carbon: experimental design optimization

M. Ghaedi[a,*], R. Hassani[b], K. Dashtian[a], G. Shafie[b], M.K. Purkait[c], H. Dehghan[b]

[a]*Chemistry Department, Yasouj University, Yasouj 75918-74831, Iran, Tel. +98 741 2223048; Fax: +98 741 2223048; emails: m_ghaedi@mail.yu.ac.ir (M. Ghaedi), dashtiankheibar@gmail.com (K. Dashtian)*
[b]*Department of Chemistry, Islamic Azad University, Marvdasht Research and Sciences Branch, Marvdasht, Iran, emails: z.hassani666@yahoo.com (R. Hassani), gshafiee2000@yahoo.com (G. Shafie), mosleh@std.yu.ac.ir (H. Dehghan)*
[c]*Department of Chemical Engineering, Indian Institute of Technology Guwahati, Guwahati 781039, Assam, India, email: mihir@iitg.ernet.in (M.K. Purkait)*

Received 9 February 2015; Accepted 4 December 2015

ABSTRACT

In this study, palladium nanoparticles were synthesized and characterized by SEM, TEM, and BET analysis. The synthesized nanoparticles were loaded on activated carbon (Pd-NP-AC) and its adsorption efficiency was measured for methyl red (MR) removal from aqueous solution. To analyze the data, an experimental design was adopted considering three operating parameters viz. initial MR concentration, adsorbent mass, and contact time as input variables while the pH was optimized using one at a time method. Statistical analysis of data corresponded to MR holds in good agreement with predicted and experimental removal percentage. The equilibrium data followed Langmuir isotherm model, while pseudo-second-order and intraparticle diffusion models cooperatively represented experimental adsorption data at various time. High adsorption capacity was obtained because of high available surface area of the nanoparticle loaded adsorbent.

Keywords: Adsorption; Methyl red; Palladium nanoparticles; Central composite design; Activated carbon

1. Introduction

Textile industries contain large amount of synthetic complex organic dyes generally intermixed with soils and water resource that are [1] carcinogenic, hazardous to reproductive organs, toxic, and neurotoxic [2]. Therefore, the removal of dye from contaminated industrial streams is highly recommended. Methyl Red (MR) swallowing or inhalation and/or skin exposure strongly affects health and safety. Electrochemical treatment [3], oxidation [4], ozonation [5], photochemical treatment [6], and froth flotation [7] are well known for the treatment of dye containing wastewater. Adsorption has overwhelming advantages over aforementioned techniques [8], and is popular for the removal of various pollutants. This technique is cheap, rapid, simple, and easy to operate [9–11]. The number of reactive sites and specific surface area may be enhanced using nanostructure material [12,13]. Activated carbon (AC) is an effective and versatile material produced from carbon-containing groups. High specific surface areas with tailored surface chemistry

*Corresponding author.

are known to be versatile materials for cleanup approaches. AC is usable for loading nanomaterial that lead to increase in adsorption capacity in shorter time to efficiently remove dye compound from dilute solution. Due to the ability to adsorb more pollutants through physical and/or chemical interaction, nanoparticle-loaded AC might be a better alternative.

Nontoxic and low-cost adsorbent are best choice for accumulation of wide range of pollutants. Composite nanoparticles such as palladium nanoparticles loaded on activated carbon (Pd-NP-AC) are a promising material with soft reactive atom in combine to AC. Reactive sites of AC and functional groups improve the performance of the adsorption system. Experimental design is an excellent tool for studying the individual and interaction effects of all parameters simultaneously [14]. The analysis in which the evaluation of more than one factor can be done is called full factorial analysis. Central composite design as particle statistical technique is a good selection for optimization of several factors which are controlled and their effects on each other are investigated at two or more levels [15]. In general, central composite design is an appropriate model based on dealing with multiple levels of several factors [16]. The capability of central composite design in the modeling of complex systems makes it more practical method than other traditional techniques for multivariable optimization instead of conventional one factor at a time [17].

In this work, palladium nanoparticles-loaded AC (Pd-NP-AC) was synthesized and subsequently characterized using different techniques such as SEM, TEM, and BET analysis. General central composite design was applied to examine factors affecting adsorption efficiency including sonication time (min), initial MR concentration (mg L^{-1}), and amount of adsorbent (mg). Then, the adsorption kinetics and isotherms of MR removal by the said adsorbent was investigated. The adsorption rates were evaluated by fitting the experimental data to traditional kinetic models such as pseudo-first- and second-order and intraparticle diffusion models. This study will be useful for quantitative adsorption of the MR in the said adsorbent with high sorption capacities in short time.

2. Experimental

2.1. Instruments and reagents

All the chemicals were used as received without further purification from Merck, dermas at, Germany. Equipment's were used according to manufacture recommendation correspond to previous publication [8–10,17,18].

2.2. Measurements of dye uptake

The MR concentrations were determined using calibration curve corresponds to maximum MR wavelength over working concentration. The efficiency of MR removal was determined at different experimental condition according central composite design.

2.3. Experimental design

A comprehensive design of experiment namely as CCD applied to evaluate the influence of operating parameters like concentration of MR (X_1), amount of adsorbent (X_2), and sonication time (X_3) are input parameters, while their influence on $R\%_{MR}$ was considered as a response was investigated and optimized. The input variables and their levels were presented in Table 1 (23 experiments). All experimental designs were executed randomly to minimize experimental errors precisely. Then, the *F*-test analysis of variance (ANOVA) at 95% confidence level was used to give idea about contribution of main factors and their interactions [18]. Design Expert 7.0 was used to analyze the experimental data according to CCD and subsequently regression model, and the response can be explained by the following first-degree polynomial equation Eq. (1):

$$Y = b_0 + \sum_{i=1}^{3} b_i x_i + \sum_{i=1}^{3} b_{ii} x_i^2 + \sum_{i=1}^{3} \sum_{j=i+1}^{3} b_{ij} x_i x_j \quad (1)$$

The adjusted R^2 is a useful unit for comparing the explanatory power of models with different numbers of predictors [19]. The smallest mean square error (MSE) [19] suggests high efficiency and applicability of model and equation for the explanation of experimental data.

2.4. Preparation of palladium nanoparticles and loaded on activated carbon

The Pd nanoparticles were synthesized in one step based on reduction of Na_2PdCl_4 in aqueous solution according to our previous reports [29]. The rate of reaction was accelerated in presence of ultrasound. Typically, Pd nanoparticle suspension was mixed with activated carbon while mixing the mixture for up to 12 h to produce Pd-NP-AC. The carbon-supported Pd nanoparticles were generally dried at 110°C under N_2-atmosphere for 1 h. A mortar was used to homogeneously ground the carbon-supported Pd nanoparti-

Table 1
Central composite design experiments and the responses obtained

Run	X_1 (Concentration of MR (mg L^{-1}))	X_2 (Adsorbent Mass (mg))	X_3 (Sonication time (min))	$R\%_{MR}$
1	15	5	10	87.81
2	15	15	15	88.24
3	9	21	7	85.17
4	15	15	10	83.33
5	21	21	7	61.23
6	15	15	10	83.33
7	15	25	10	66.46
8	5	15	10	78.82
9	21	9	7	76.13
10	15	15	5	75.03
11	15	15	10	83.33
12	9	21	13	80.05
13	21	9	13	87.11
14	25	15	10	71.75
15	15	15	10	90.92
16	15	15	10	90.92
17	15	15	10	90.92
18	15	15	10	90.92
19	21	21	13	70.45
20	9	9	7	84.13
21	9	9	13	98.35
22	15	5	10	87.81
23	15	15	15	88.24

cles powders. The carbon-supported Pd nanoparticles were stored in air at room temperature and were found to have a shelf life of at least 1 year.

3. Results and discussion

3.1. Characterization of adsorbent

UV–vis analysis depicts the maximum wavelength at 245 and 290 nm for Na_2PdCl_4 in aqueous media. These were because of reasonable sensitivity due to ligand-to-metal charge transfer and/or the hydrolysis product of $PdCl_3(H_2O)^-$ [20,21]. It was found that the sensitivity strongly diminished and led to appearance of dark brown color. The dark brown color of the solution showed indication of the formation of Pd nanoparticles suspension which has no SPR in the visible region (Fig. 1). This indicates that the ascorbic acid serves as both reducing and antioxidant agent. The SEM images of the activated carbon surface and the Pd nanoparticles deposited on activated carbon are shown in (Figs. 2(a) and (b)). The images show the formation of more porous adsorbent following Pd-NP deposition on AC without agglomeration The diameter of Pd nanoparticles are in the range of 20–60 nm. The particle size measured directly from this SEM image agrees with respective estimated value of TEM

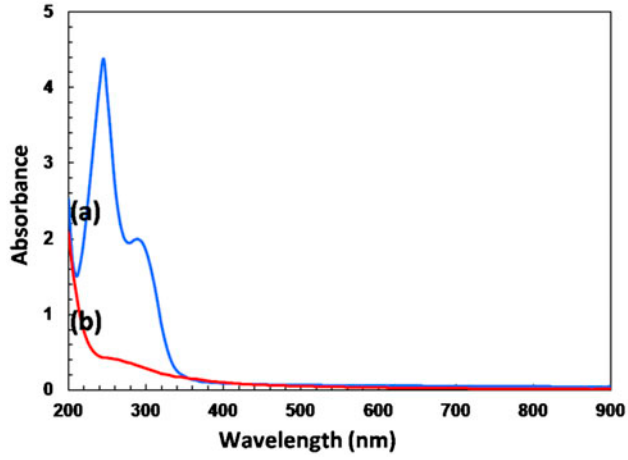

Fig. 1. UV–vis absorbance spectra of (a) aqueous Na_2PdCl_4 solution and (b) Pd nanoparticles suspension.

image (Fig. 2(c)). This confirms narrow particle size distribution (25–90 nm). Exact crystal structure of the Pd nanoparticles, diffraction rings of the Pd nanoparticles ED pattern (Fig. 2(d)) reveal cubic structure. The rings in electron diffraction pattern can be assigned to the [1 1 1], [2 0 0], [2 2 0], [3 1 1], and [2 2 2] crystal planes of a face-centered cubic (FCC) lattice structure

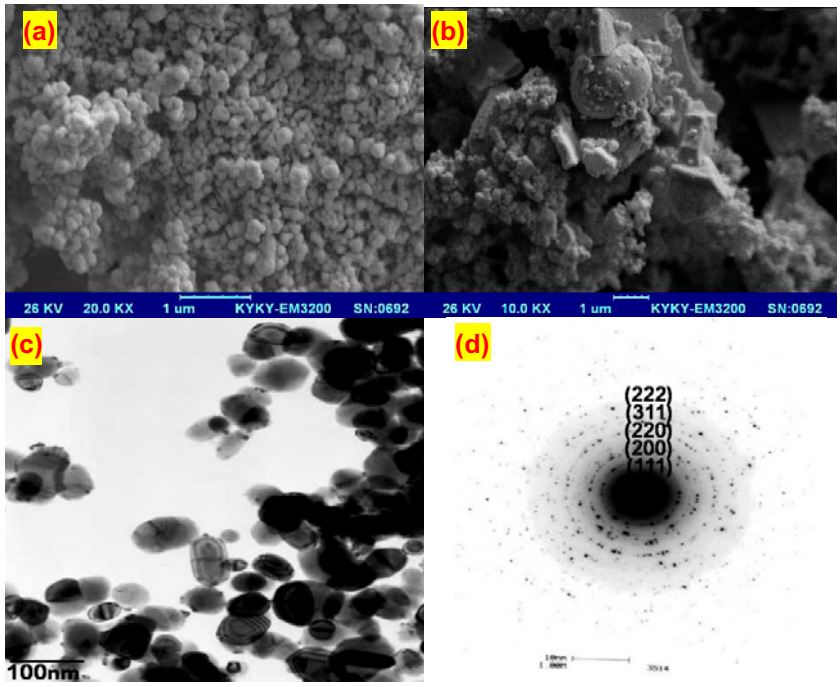

Fig. 2. SEM images of (a) the activated carbon and (b) the Pd nanoparticles deposited on activated carbon and typical TEM image of the starch-stabilized Pd nanoparticles (c) and the electron diffraction (ED) pattern of the Pd nanoparticles (d).

of the Pd nanoparticles [22,23]. The BET surface area of AC and Pd-NPs loaded on AC was measured and shown in Table 2. A high surface area (1,340.07 m^2/g) of Pd-NP-AC makes it suitable as a very good adsorbent.

3.2. Effect of pH

The pH is one of the most important parameters in controlling the adsorption process and is shown in Fig. 3. It revealed that minimum and maximum MR removal was achieved at pH 7 and 2, respectively. Its appearance changes due to formation of different ionic species at pH change, while main mechanism is soft–hard theory which is accelerated by presence of hydrogen bonding. MR adsorption on Pd-NPAC is soft–soft interaction with palladium atom of adsorbent or hydrogen bonding with various functional group of AC. At lower pH, the electrostatic attraction force among functional groups of AC and MR molecules cause Increase in MR removal percentage. At pH value higher than 2, the existence of Pd-NP-AC sur-

Table 2
Information obtained by BET taken from Pd nanoparticles on activated carbon

Summary report	Pd-NP-AC
BET surface area	1,340.07 m/g
Langmuir surface area	1,838.16 m/g
BJH Adsorption cumulative surface area of pores between 17.000 and 3,000.000 Å width	154.31 m/g
BJH Desorption cumulative surface area of pores between 17.000 and 3,000.000 Å width	180.01 m/g
BJH Adsorption cumulative volume of pores between 17.000 and 3,000.000 Å width	13.95×10^{-2} cm/g
BJH Desorption cumulative volume of pores between 17.000 and 3,000.000 Å width	14.87×10^{-2} cm/g
t-Plot micropore volume	23.74×10^{-2} cm/g
Adsorption average pore width (4 V/A by BET)	20.07 Å
BJH Adsorption average pore width (4 V/A)	36.16 Å
BJH Desorption average pore width (4 V/A)	33.063 Å

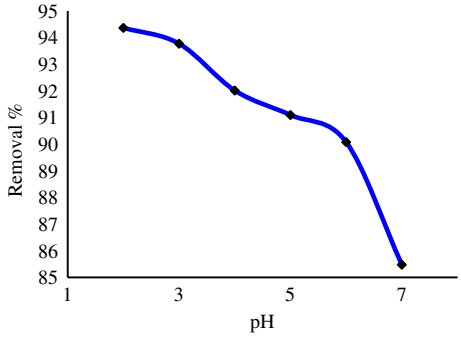

Fig. 3. Effect of pH on $R\%_{MR}$ at range of 2–7.

face OH^- creates a competition between ionic dye and decreases the aggregation of MR [24,25].

3.3. Statistical analysis

Main effect of factors and their interactions for influencing removal percentage of MR was studied using ANOVA. The *p*-value, *F*-value, sum of squares, and mean square of each factor were represented in Table 3. The *p*-value and *F*-value closer to zero depicts the greater significance. To consider statistical significance of 95% confidence level, the *p*-value should be less than or equal to 0.05 [26]. According to the obtained *F*-value and *p*-value from ANOVA, the effects of main variables and their dyadic interaction are statistically significant. These parameters were characterized by a greater degree of departure from the overall which means sonication time (X_3), adsorbent mass (X_2), and MR concentration (X_1) had a significant effect on removal percentage of MR. Based on these results, an empirical relationship between the $R\%_{MR}$ and input variables was proposed by the following polynomial equation:

$$R\%_{MR} = 87.02 - 5.4X_1 - 5.54X_2 + 3.12X_3 - 4.95X_1X_2 + 0.03XX_1X_3 - 3.65X_2X_3 - 3.95X_1^2 - 1.76X_2^2 - 0.17X_3^2 \quad (2)$$

The output results from the model indicated good agreement between the experimental and predicted values of $R\%_{MR}$. As well as determination of coefficient $R^2 = 0.98$, and adjusted $R^2 = 0.96$ can be well predicted by the model, indicating that the terms which was considered in the proposed model are significant enough to make acceptable predictions. However, adding more terms improve the model predictions. Indeed, the high *F*-value (55.4) confirms the significance of the proposed model. The experimental and predicted $R\%_{MR}$ is shown in Fig. 4. Actual values are the measured data for a specific run, and the predicted values were evaluated from the model, and generated using the approximated function. In accordance with a high percentage of the obtained correlation coefficient, the model is a satisfactory fit to the experimental data.

3.4. 3D surface plots

3D surface plots were used to guess the variables participant as sole or interactive (Fig. 5). These plots were obtained for a given pair of actual factors at fixed and central values of other variables. The effect of adsorbent dosage on the $R\%_{MR}$ (Fig. 5(a) and (c)), indicated that lower adsorbent mass led to reduction

Table 3
ANOVA for the quadratic model applied for removal of MR

Source of variation	Degree freedom	Sum of square	Mean square	*F*-value	*p*-value
Model	9	1,483.00	199.69	55.60	<0.0001
X_1	1	360.66	164.78	121.70	<0.0001
X_2	1	411.96	360.66	139.01	<0.0001
X_3	1	130.77	411.96	44.13	<0.0001
X_1X_2	1	143.46	130.77	48.41	<0.0001
X_1X_3	1	0.71	143.46	0.24	0.6351
X_2X_3	1	105.86	0.71	35.72	0.0001
X_1^2	1	235.08	105.86	79.32	<0.0001
X_2^2	1	41.70	235.08	14.07	0.0038
X_3^2	1	0.39	41.70	0.13	0.7229
Residual	10	29.64	0.39		
Lack of fit	5	29.64	2.96		
Pure error	5	0.000	5.93		
Cor. total	20	1,712.33			

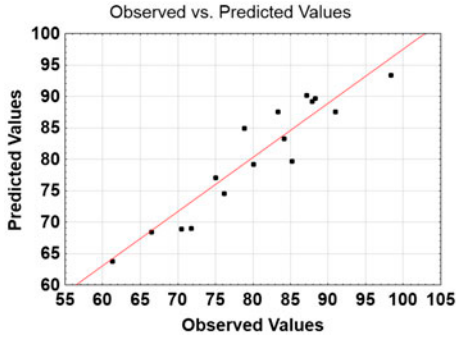

Fig. 4. Experimental vs. predicted $R\%_{MR}$.

in removal percentage due to unbalancing the dyes molecules to vacant sites of Pd–NP-AC, while at higher value reverse behavior was seen. The effect of initial MR concentration on the $R\%_{MR}$ (Fig. 5(a) and (b)) reveals that at lower value, high removal percentage was observed because of more available adsorption site, while reverse trend was seen at higher MR concentration. The effect of contact time on the $R\%_{MR}$ (Fig. 5(b) and (c)) suggests that short equilibrium time emerged from acceleration of mass transfer and well mixing adsorbent with bulk solution that lead to high available surface area and vacant sites of adsorbent is enhanced by ultrasonic power. The mass transfer due to raising diffusion coefficient encounter enhance in rate.

3.5. Adsorption equilibrium study

Adsorption equilibrium isotherm represents mathematical relation of amount of adsorbed target per gram of adsorbent (q_e (mg g^{-1})) to the equilibrium solution concentration (C_e (mg/L)) at fixed temperature. The data obtained during equilibrium study has been fitted to various adsorption isotherm equations such as Langmuir, Freundlich, Temkin, and Dubinin–Radushkevich (D–R) isotherms to discuss the equilibrium characteristics of the adsorption process [27,28]. The constant parameters and correlation coefficients (R^2) obtained from the plots of known equation for Langmuir, Freundlich, Temkin, and D–R are summarized in Table 4. The fitness investigation of experimental data was at some different level of adsorbent mass. High correlation coefficient Langmuir model at all conditions suggests its good ability in interpretation of the experimental data over the whole concentration range. The values of $1/n$ for Freundlich isotherm shows the high tendency of MG for the adsorption onto AC, while lower R^2 value show its unsuitability for fitting the experimental data over the

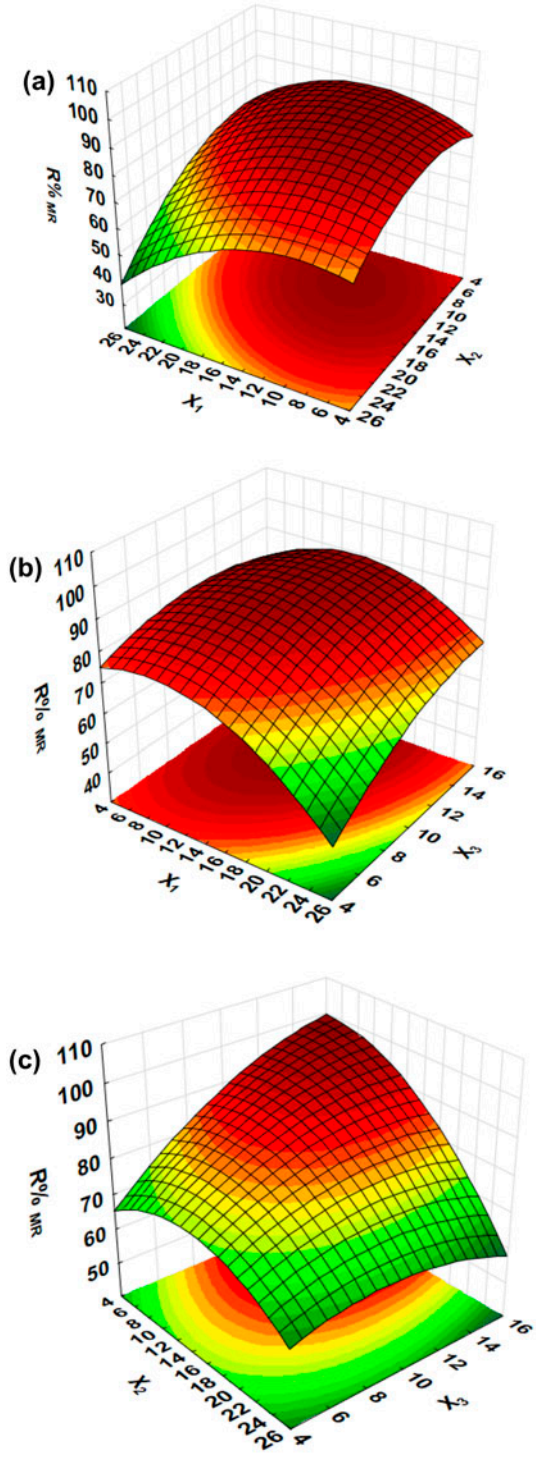

Fig. 5. 3D response surface plots.

whole concentration range. Based on the Temkin isotherm model, the heat of the adsorption and the adsorbent–adsorbate interaction were evaluated. The values of the Temkin constants and the correlation

Table 4
Isotherm constants of MR adsorption onto Pd-NP-AC

Adsorbent (mg) Isotherm	Equation	Parameters	10	15	20
Langmuir	$C_e/q_e = 1/K_aQ_m + q_e/Q_m$	Q_m (mg g^{-1})	133.33	72.99	60.97
		K_a (L mg^{-1})	2.77	2.74	1.50
		R^2	0.98	0.99	0.99
Freundlich	$\ln q_e = \ln K_F + (1/n) \ln C_e$	$1/n$	4.14	4.54	4.06
		K_F (L mg^{-1})	77.03	40.08	31.08
		R^2	0. 87	0.89	0.93
Temkin	$q_e = B_1 \ln K_T + B_1 \ln C_e$	B_1	34.16	32.25	33.73
		K_T (L mg^{-1})	49.89	80.62	103.52
		R^2	0.89	0.91	0.91
Dubinin–Radushkevich	$\ln q_e = \ln Q_s - K\varepsilon^2$	Q_s (mg g^{-1})	97.50	51.92	36.23
		K	-2×10^{-6}	-2×10^{-7}	-2×10^{-7}
		E (J/mol) = $1/(2\ K)^{1/2}$	500	500	7,090
		R^2	0.87	0.91	0.91

Table 5
Kinetic parameters of MR adsorption onto Pd-NP-AC. Conditions: 10 mg adsorbent over 10–100 mg L^{-1} at optimal conditions of other variables

	Parameter values: concentration dye (mg L^{-1})					
Models	Parameters	10	20	40	50	100
First-order-kinetic model						
$\log(q_e - q_t) = \log(q_e) - (K_1/2.303)t$	K_1	0.217	0.121	0.190	0.179	0.110
	$q_{e(cal)}$	10.16	20.43	57.32	127.32	321.22
	R^2	0.91	0.86	0.79	0.93	0.81
Second-order-kinetic model						
$t/q_t = 1/k_2q_e^2 + (1/q_e)t$	K_2	0.055	0.017	0.004	0.009	0.004
	$q_{e(cal)}$	50.76	101.01	208.33	212.77	344.83
	R^2	0.99	0.99	0.99	0.99	0.99
	h	141.71	173.45	173.61	407.44	475.63
Intraparticle diffusion						
$q_t = K_{id}t^{1/2} + C$	K_{dif}	8.72	7.31	7.31	21.75	21.75
	C	33.123	38.87	38.87	15.52	15.52
	R^2	0.841	0.778	0.778	0.972	0.972
Elovich	α	456.82	569.44	586.30	189.23	586.30
$q_t = 1/\beta \ln(\alpha\beta) + 1/\beta \ln(t)$	β	0.098	0.098	0.098	0.067	0.067
	R^2	0.96	0.94	0.94	0.97	0.97
Experimental data	$Q_{e(exp)}$	49.917	99.91	199.91	249.91	499.91

coefficient are lower than the Langmuir value. Another adsorption isotherm such as D–R model was applied to estimate the porosity apparent free energy and the characteristic of adsorption. The mean free energy of the adsorption (E) was calculated, while lower value of correlation coefficient corresponding to

this model denotes its failure for representation of experimental data. In this case, the D–R equation represents the poorer fit of the experimental data than the other isotherm equations. Among various isotherms model, the best usable model is Langmuir as variation of adsorbent and adsorbate gets hinder from multilayer adsorption.

3.6. Adsorption kinetic modeling

Four kinetic models such as pseudo-first- and second-order, Elovich and intraparticle diffusion model with well known and general conditions are able to interpret the rate and mechanism of each adsorption process. The prediction of adsorption kinetics is necessary for the design of industrial adsorption model. The nature of the adsorption process will depend on physical or chemical characteristics of the adsorbent and the system conditions. The experimental kinetic data of MR were correlated by such kinetic models including pseudo-first- and second-order, Elovich, and intraparticle diffusion to study the rate and mechanism of an adsorption process. Table 5 summarized the properties of each model. The experimental adsorption data at some initial MR concentration (10 and 100 mg L^{-1}) and 10 mg of adsorbent was examined and experimental data are presented in Table 5. Distance of intercept from experimental q_e value is an indication of low ability of this model to explain experimental data and denotes that rate of adsorption does not follow from this equation [29]. The sorption kinetics may be described by a pseudo-second-order model [30]. The R^2 value for pseudo-second-order kinetic model was found to be higher (0.99) and the calculated q_e value is close to the experimental adsorption capacity value under different physicochemical conditions (Table 5). The Elovich equation is based on the adsorption capacity in linear form also applied for the adsorption of MR from a solution Pd-NP-AC [31]. The plot of q_t vs. ln (t) should yields a linear relationship with a slope of ($1/\beta$) and an intercept of ($1/\beta$) ln ($\alpha\beta$). The Elovich constants obtained from the slope and the intercept of the straight line are reported in Table 5. The correlation coefficient is higher than 0.98 shows the suitability of the model for evaluation of the adsorption process. The later process possibility is explored using the intraparticle diffusion model based on diffusive mass transfer that adsorption rate expressed in terms of the square root of time (t) [32]. The values of K_{diff} and C were calculated from the slope and intercept of the plot of q_t vs. $t^{1/2}$. C value is related to the thickness of the boundary layer and K_{diff} is the intraparticle diffusion rate constant (mg g^{-1} $min^{-1/2}$). The values of K_{diff} and C were obtained from the final linear portion and their values are presented in Table 5. Since the intraparticle curve did not pass through the origin; one can notice that apart from intraparticle diffusion model another stage such as second-order kinetic model can control the adsorption process.

4. Conclusion

The present study reveals that Pd-NP-AC is an efficient material for fast and quantitative removal of MR. The influences of experimental parameters on the removal percentage of MR were investigated by CCD. The Langmuir isotherm explained equilibrium data very well. The adsorption kinetics was successfully fitted with the pseudo-second-order kinetic model. A high correlation coefficient (R^2 = 0.98) ensured the satisfactory adjustment of the proposed model to the experimental data. Finally, the Pd-NP-AC may be used as an efficient adsorbent for the removal of MR.

Acknowledgments

The authors thanks of the Research Council of the Yasouj University for financial supporting this work.

References

[1] A.M. Talarposhti, T. Donnelly, G.K. Anderson, Colour removal from a simulated dye wastewater using a two-phase Anaerobic packed bed reactor, Water Res. 35 (2001) 425–432.
[2] S. Çoruh, E.H. Gurkan, Adsorption of neutral red from aqueous solutions using waste foundry sand: Full factorial design analysis, Environ. Prog. Sustain. Energy 33 (2014) 1086–1095.
[3] S. Çoruh, F. Geyikçi, S. Elevli, Adsorption of neutral red dye from an aqueous solution onto natural sepiolite using full factorial design, Clay Clay Miner. 57 (2011) 617–625.
[4] A. Özcan, M.A. Oturan, N. Oturan, Y. Sahin, Removal of Acid Orange 7 from water by electrochemically generated Fenton's reagent, J. Hazard. Mater. 163 (2009) 1213–1220.
[5] K.P. Singh, S. Gupta, A.K. Singh, S. Sinha, Optimizing adsorption of crystal violet dye from water by magnetic nanocomposite using response surface modeling approach, J. Hazard. Mater. 186 (2011) 1462–1473.
[6] A. Sari, D. Mendil, M. Tuzen, M. Soylak, Biosorption of Cd(II) and Cr(III) from aqueous solution by moss (*Hylocomium splendens*) biomass: Equilibrium, kinetic and thermodynamic studies, Chem. Eng. J. 144 (2008) 1–9.
[7] S. Koru, S. Elevli, Optimization of malachite green dye removal by sepiolite clay using a central composite design, Global NEST J. 16 (2014) 340–348.

[8] M. Ghaedi, A. Ansari, F. Bahari, A.M. Ghaedi, A. Vafaei, A hybrid artificial neural network and particle swarm optimization for prediction of removal of hazardous dye brilliant green from aqueous solution using zinc sulfide nanoparticle loaded on activated carbon, Spectrochim. Acta Part A: Mol. Biomol. Spectrosc. 137 (2015) 1004–1015.
[9] M. Ghaedi, A. Ansari, R. Sahraei, ZnS: Cu nanoparticles loaded on activated carbon as novel adsorbent for kinetic, thermodynamic and isotherm studies of Reactive Orange 12 and Direct yellow 12 adsorption, Spectrochim. Acta Part A: Mol. Biomol. Spectrosc. 114 (2013) 687–694.
[10] M. Ghaedi, A.M. Ghaedi, A. Ansari, F. Mohammadi, A. Vafaei, Artificial neural network and particle swarm optimization for removal of methyl orange by gold nanoparticles loaded on activated carbon and Tamarisk, Spectrochim. Acta Part A: Mol. Biomol. Spectrosc. 132 (2014) 639–654.
[11] V. Meshko, L. Markovska, M. Mincheva, A.E. Rodrigues, Adsorption of basic dyes on granular activated carbon and natural zeolite, Water Res. 35 (2001) 3357–3366.
[12] M. Ghaedi, F. Mohammdi, A. Ansari, Gold nanoparticles loaded on activated carbon as novel adsorbent for kinetic and isotherm studies of methyl orange and sunset yellow adsorption, J. Dispersion Sci. Technol. 36 (2015) 652–659.
[13] J. Bajpai, R. Shrivastava, A.K. Bajpai, Dynamic and equilibrium studies on adsorption of Cr(VI) ions onto binary bio-polymeric beads of cross linked alginate and gelatin, Colloids Surf., A: Physicochem. Eng. Aspects 236 (2004) 81–90.
[14] D. Bingol, N. Tekin, M. Alkan, Brilliant Yellow dye adsorption onto sepiolite using a full factorial design, Appl. Clay Sci. 50 (2010) 315–321.
[15] M. Ravanan, M. Ghaedi, A. Ansari, F. Taghizadeh, D. Elhamifar, Comparison of the efficiency of Cu and silver nanoparticle loaded on supports for the removal of Eosin Y from aqueous solution: Kinetic and isotherm study, Spectrochim. Acta Part A: Mol. Biomol. Spectrosc. 123 (2014) 467–472.
[16] M.E.R. Carmona, M.A.P. da Silva, S.G.F. Ferreira Leite, Biosorption of chromium using factorial experimental design, Process Biochem. 40 (2005) 779–788.
[17] M. Jamshidi, M. Ghaedi, K. Dashtian, S. Hajati, A. Bazrafshan, Ultrasound-assisted removal of Al^{3+} ions and Alizarin red S by activated carbon engrafted with Ag nanoparticles: Central composite design and genetic algorithm optimization, RSC Adv. 5 (2015) 59522–59532.
[18] F.N. Azad, M. Ghaedi, K. Dashtian, M. Montazerozohori, S. Hajati, E. Alipanahpour, Preparation and characterization of MWCNTs functionalized by N-(3-nitrobenzylidene)-N´-trimethoxysilylpropyl-ethane-1,2-diamine for the removal of aluminum(iii) ions via complexation with eriochrome cyanine R: Spectrophotometric detection and optimization, RSC Adv. 5 (2015) 61060–61069.
[19] D.C. Montgomery, Design and Analysis of Experiments. Minitab Manual, John Wiley & Sons, New York, 2011.
[20] Q. Zhang, J. Xie, J. Yang, J.Y. Lee, Monodisperse icosahedral Ag, Au, and Pd nanoparticles: Size control strategy and superlattice formation, ACS Nano 3 (2009) 139–148.
[21] Y.W. Lee, N.H. Kim, K.Y. Lee, K. Kwon, M. Kim, S.W. Han, Synthesis and characterizationof flower-shaped porous Au-Pd alloy nanoparticles, J. Phys. Chem. C 112 (2008) 6717–6722.
[22] B. Lim, M. Jiang, J. Tao, P.H.C. Camargo, Y. Zhu, Y. Xia, Shape-controlled synthesis of Pd nanocrystals in aqueous solutions, Funct. Mater. Lett. 1 (2008) 1–6.
[23] M. Ghaedi, A.M. Ghaedi, M. Hossainpour, A. Ansari, M.H. Habibi, A.R. Asghari, Least square-support vector (LS-SVM) method for modeling of methylene blue dye adsorption using copper oxide loaded on activated carbon: Kinetic and isotherm study, J. Ind. Eng. Chem. 20 (2014) 1641–1649.
[24] M. Ghaedi, A.M. Ghaedi, E. Negintaji, A. Ansari, A. Vafaei, M. Rajabi, Random forest model for removal of bromophenol blue using activated carbon obtained from *Astragalus bisulcatus* tree, J. Ind. Eng. Chem. 20 (2014) 1793–1803.
[25] M. Roosta, M. Ghaedi, A. Daneshfar, R. Sahraei, A. Asghari, Optimization of combined ultrasonic assisted/tin sulfide nanoparticle loaded on activated carbon removal of erythrosine by response surface methodology, J. Ind. Eng. Chem. 21 (2015) 459–469.
[26] P. Assefi, M. Ghaedi, A. Ansari, M.H. Habibi, M.S. Momeni, Artificial neural network optimization for removal of hazardous dye Eosin Y from aqueous solution using Co_2O_3-NP-AC: Isotherm and kinetics study, J. Ind. Eng. Chem. 20 (2014) 2905–2913.
[27] A. Shamsizadeh, M. Ghaedi, A. Ansari, S. Azizian, M.K. Purkait, Tin oxide nanoparticle loaded on activated carbon as new adsorbent for efficient removal of malachite green-oxalate: Non-linear kinetics and isotherm study, J. Mol. Liquids 195 (2014) 212–218.
[28] M. Ghaedi, H. Khajesharifi, A. Hemmati Yadkuri, M. Roosta, R. Sahraei, A. Daneshfar, Cadmium hydroxide nanowire loaded on activated carbon as efficient adsorbent for removal of Bromocresol Green, Spectrochim. Acta Part A: Mol. Biomol. Spectrosc. 86 (2012) 62–68.
[29] S. Arabzadeh, M. Ghaedi, A. Ansari, F. Taghizadeh, M. Rajabi, Comparison of nickel oxide and palladium nanoparticle loaded on activated carbon for efficient removal of methylene blue: Kinetic and isotherm studies of removal process, Hum. Exp. Toxicol. 34(2) (2015) 153–169.
[30] M. Sheibani, M. Ghaedi, F. Marahel, A. Ansari, Congo red removal using oxidized multiwalled carbon nanotubes: Kinetic and isotherm study, Desalin. Water Treat. 53 (2015) 844–852.
[31] M. Ghaedi, A. Ansari, M.H. Habibi, A.R. Asghari, Removal of malachite green from aqueous solution by zinc oxide nanoparticle loaded on activated carbon: Kinetics and isotherm study, J. Ind. Eng. Chem. 20 (2014) 17–28.
[32] M. Roosta, M. Ghaedi, A. Asfaram, Simultaneous ultrasonic-assisted removal of malachite green and safranin O by copper nanowires loaded on activated carbon: Central composite design optimization, RSC Adv. 5 (2015) 57021–57029.